

THE RAMAN STUDY OF SINGLE-CHAIN SILICATES

ANDREI BUZATU¹, NICOLAE BUZGAR¹

¹ “Al. I. Cuza” University of Iași, Department of Geology, 20A Carol I Blv.,
700505 Iași, Romania

Abstract

Some of the most common pyroxenes (bronzite, hypersthene, diopside, hedenbergite, augite, omphacite, aegirine and spodumene) and pyroxenoids (wollastonite, rhodonite, fowlerite and charoite) have been investigated by non-contact Raman spectroscopy. In order to complete the information on the vibrational modes, the IR spectrum of augite was devised. In the Raman spectrum of aegirine, the bands appear at lower wavenumbers than in the rest of the pyroxenes. The bands assigned to the Si-O vibrational modes are split due to the deformation of the tetrahedra. In the rhodonite and zinc-rich variety (fowlerite) spectra, differences were noted; in fowlerite, some bands are shifted at higher frequencies, compared with rhodonite. The pyroxenoids presented the same typical bands of the single-chain structure. The spectrum of charoite shows two new lines at 2367 cm⁻¹ and 2403 cm⁻¹, which are due to the modes of the N-H bonds.

Key words: Raman spectra, IR, pyroxenes, pyroxenoids, single-chain silicates, aegirine, fowlerite, charoite.

Introduction

Pyroxenes are one of the most abundant rock-forming minerals on Earth (Deer et al., 1997). Studies showed that these minerals are also the major silicates on the surface of Mars (Wang et al., 2001). Many Raman studies on pyroxenes and pyroxenoids were made (Etchepare, 1971; Sharma et al., 1983; McMillan, 1984; Mernagh and Hoatson, 1997; Swamy et al., 1997; Huang et al., 2000; Mills et al., 2004; Pommier et al., 2005; Makreski

¹ e-mail: andrei.buzatu@geology.uaic.ro

et al., 2006; Katerinopoulou et al., 2007), but less information was found about aegirine and charoite minerals.

The structure of pyroxenes is built up by the linkage of SiO_4 tetrahedra sharing two out of four corners forming continuous chains along the *c* axis. Two tetrahedra repeat in these chains. Cations are located between them, in sites labelled *M1* and *M2*. Pyroxenes include two groups: orthopyroxenes (orthorhombic symmetry) and clinopyroxenes (monoclinic symmetry). When the cation in the *M2* site is six-fold coordinated, the minerals are orthorhombic (enstatite-ferrosilite), and when it is in eight-fold coordination they are monoclinic. In clinopyroxenes, the *M2* site is occupied by Ca^{2+} , Na^+ , Li^+ cations (diopside, hedenbergite, augite, aegirine, spodumene). The *M1* site is six-fold coordinated and occupied by Fe^{3+} , Al^{3+} , Fe^{2+} , Mg^{2+} , Mn^{2+} . The orthopyroxenes studied for the present paper (bronzite and hypersthene) have a *Pbca* structure, and the clinopyroxenes are in the *C2/c* space group, except for omphacite, which is *P2/n* (Deer et al., 1997). The pyroxenoid structure consists of the same type of SiO_4 chains, but the repeating unit of the tetrahedra is 3 (wollastonite), 5 (rhodonite) or higher. The pyroxenoids studied in this paper are wollastonite, rhodonite, fowlerite (triclinic) and charoite (monoclinic). Fowlerite is the zinc-rich variety of rhodonite. The charoite structure consists in pectolite-like chains of SiO_4 tetrahedra between bands of Ca polyhedra, with tubular structures where K atoms and H_2O molecules are situated (Rozhdestvenskaya et al., 2009).

The Raman spectra of single-chain silicates are characterized by four types of vibrations: (1) Si-O nonbridging stretching (Si-O_{nbr}); (2) Si-O bridging stretching (Si-O_{br}); (3) O-Si-O bending; and (4) cation-oxygen vibration modes (M-O). The stretching modes of Si-O_{nbr} are observed in the spectra at frequencies higher than the modes of Si-O_{br} , due to a stronger force constant (in the case of Si-O_{br} bonds, the force constant is shared between the adjacent tetrahedra) (Sharma et al., 1983; McMillan, 1984; Mernagh and Hoatson, 1997; Huang et al., 2000; Katerinopoulou et al., 2007).

Analytical procedure

The Raman spectra were obtained at room temperature with a Horiba Jobin-Yvon RPA-HE 532 Raman Spectrograph with multichannel air cooled (-70°C) CCD detector, using a wavenumber doubled Nd-Yag laser, 532 nm and nominal power 100 mW. The spectral resolution was 3 cm^{-1} and the spectral range – between 200 and 3400 cm^{-1} . The Raman system includes a “Superhead” optic fibre Raman probe for non-contact measurements, with an Olympus 50X LWD visible objective, $\text{NA} = 0.50$ $\text{WD} = 10.6\text{ mm}$. The sulfur and cyclohexane bands were used for the calibration of the frequencies of the Raman spectra. Data acquisition was performed through a 2 - 40 seconds exposure, 20 – 100 acquisitions, at a laser magnification of 90 – 100%, in order to improve the signal-to-noise ratio. Spectra manipulation consists in a basic treatment, such as baseline adjustment and peak fitting (Lorentz function). The figures in the current paper present the spectra in the $200\text{-}1500\text{ cm}^{-1}$ region for the minerals where no bands were observed at higher frequencies.

The IR spectrum of augite was collected with a Bruker Vertex 70 FTIR spectrometer with a spectral resolution of 2 cm^{-1} . The spectra were obtained in the spectral range

between 370-7000 cm^{-1} . The measurements were taken at room temperature, using the KBr pellet technique. The spectrum was analyzed with OPUS software.

Tab. 1 Samples used in the present study

| No. | Mineral | Formula | Sample | Origin |
|-----------------------|--------------|--|--------|----------------------------|
| <i>Pyroxenes</i> | | | | |
| <i>Magnesium-Iron</i> | | | | |
| 1. | Hypersthene | $(\text{Mg, Fe}^{2+})_2\text{Si}_2\text{O}_6$ | 5798 | St. Paul, Labrador, Canada |
| 2. | Bronzite | | 5796 | Leutunggraben, Austria |
| <i>Calcium</i> | | | | |
| 3. | Diopside | $\text{CaMgSi}_2\text{O}_6$ | 5791 | Zermatt, Switzerland |
| 4. | Diopside | | 5790 | Zillerthel, Tirol, Austria |
| 5. | Hedenbergite | $\text{CaFe}^{2+}\text{Si}_2\text{O}_6$ | 5792 | Nordmasken, Sweden |
| 6. | Hedenbergite | | 5799 | Nordmarken, Sweden |
| 7. | Augite | $(\text{Ca, Mg, Fe, Ti, Al})_2(\text{Si, Al})_2\text{O}_6$ | 3974 | Germany |
| 8. | Augite | | - | Techereu, Romania |
| <i>Calcium-Sodium</i> | | | | |
| 9. | Omphacite | $(\text{Ca, Na})(\text{Mg, Fe}^{2+}, \text{Al})\text{Si}_2\text{O}_6$ | - | South Carpatians, Romania |
| <i>Sodium</i> | | | | |
| 10. | Aegirine | $\text{NaFe}^{3+}\text{Si}_2\text{O}_6$ | 5805 | Brewig, Norway |
| 11. | Aegirine | | 5820 | Kangerdluarsuk, Greenland |
| <i>Lithium</i> | | | | |
| 12. | Spodumene | $\text{LiAlSi}_2\text{O}_6$ | 5876 | Conțu, Romania |
| <i>Pyroxenoids</i> | | | | |
| 13. | Wollastonite | CaSiO_3 | 5734 | Ciclova, Banat, Romania |
| 14. | Rhodonite | $(\text{Mn, Fe}^{2+}, \text{Mg, Ca})\text{SiO}_3$ | 5760 | Sverdlovsk, Urali, Russia |
| 15. | Fowlerite | $(\text{Mn, Zn})\text{SiO}_3$ | 5745 | Franklin, New Jersey, USA |
| 16. | Charoite | $\text{K}(\text{Ca, Na})_2\text{Si}_4\text{O}_{10}(\text{OH, F})\cdot\text{H}_2\text{O}$ | 5867 | Yakutia, Russia |

Samples

The samples used in the study are listed in table 1 and are monocrystals belonging to the „Grigore Cobălcescu” Mineralogy and Petrography Museum of the „Al. I. Cuza” University of Iași (with the exception of the augite and omphacite samples).

Results and discussions

Magnesium-Iron pyroxenes

The Raman spectra of the orthopyroxene samples studied are shown in figure 1 and the bands are listed in table 2, compared with the values obtained by Huang et al. (2000).

In theory, orthopyroxenes have 240 vibration modes: $30A_{1g}(\text{R}) + 30B_{1g}(\text{R}) + 30B_{2g}(\text{R}) + 30B_{3g}(\text{R}) + 30A_{1u} + 30B_{1u}(\text{IR}) + 30B_{2u}(\text{IR}) + 30B_{3u}(\text{IR})$ (R – Raman; IR – infrared) (Chopelas, 1999). Fewer modes were observed in our Raman spectra.

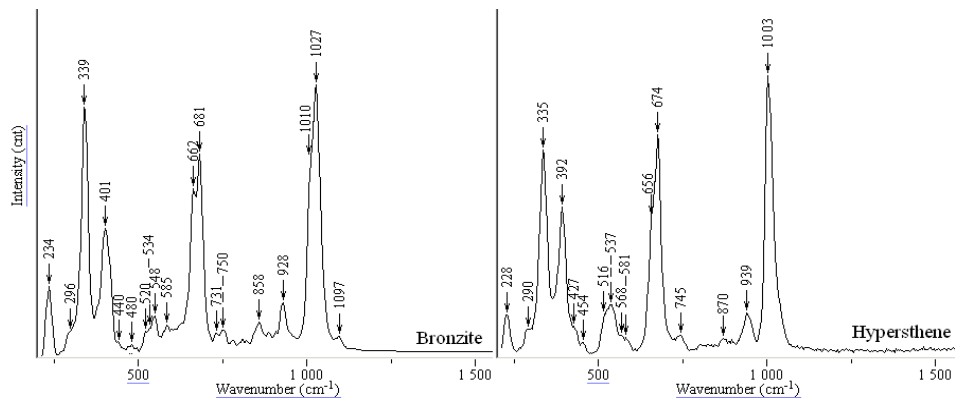


Fig. 1 Raman spectra of orthopyroxenes

Both spectra are dominated by intense bands, 1003 cm^{-1} in hypersthene and 1010 cm^{-1} and 1027 cm^{-1} in bronzite, assigned to the symmetric stretching of Si-O_{nbr} bonds. The same assignment is made for the 870 cm^{-1} and 939 cm^{-1} bands in hypersthene, and 858 cm^{-1} , 928 cm^{-1} and 1097 cm^{-1} in bronzite. In bronzite, the 1027 cm^{-1} band is more intense than the 1010 cm^{-1} one. The intensity of the peaks may vary with the orientation of the crystal (Huang et al., 2000). The $650\text{--}750\text{ cm}^{-1}$ region is assigned to the symmetric stretching of Si-O_{br} . The stronger mode from this region appears as two peaks (662 cm^{-1} and 681 cm^{-1} in bronzite; 656 cm^{-1} and 674 cm^{-1} in hypersthene) due to the *Pbca* structure which has two symmetrically distinct tetrahedral chains. The peaks between $500\text{--}600\text{ cm}^{-1}$ are attributed to the O-Si-O bending modes. The bands below 500 cm^{-1} are due to the vibration modes of M-O bonds (Huang et al., 2000).

Both hypersthene and bronzite spectra are similar, with small variations of the peak positions. Huang et al. (2000) showed that these variations in enstatite-ferrosilite series are due to the Fe^{2+} content. The wavenumbers of the Raman bands decrease with the increasing of Fe concentration (from enstatite to ferrosilite), with the exception of the $\sim 860\text{ cm}^{-1}$ and $\sim 930\text{ cm}^{-1}$ bands, where a positive correlation is observed (tab. 2). This characteristic appears in our spectra, as well. A few more weak bands were observed in the present study: in bronzite – 480 cm^{-1} , 585 cm^{-1} , 731 cm^{-1} and 1097 cm^{-1} , and in hypersthene – 290 cm^{-1} , 427 cm^{-1} , 454 cm^{-1} and 581 cm^{-1} . The hypersthene bands of 406 cm^{-1} and 1013 cm^{-1} , reported by Huang et al. (2000), were not observed in our spectra.

In orthopyroxene spectra, the wavenumbers of the Raman bands decrease with the increasing of the Fe concentration (from enstatite to ferrosilite), caused by the slightly greater size of the Fe^{2+} cation, compared to that of the Mg^{2+} . The frequency of a Raman band is determined by the bond strength and the atomic mass, the frequency increasing with the increasing of the bond strength. Atoms with small ionic radius form shorter bonds, therefore the bonds will have greater strength. $\text{Mg}^{2+}\text{-O}$ bonds are stronger than $\text{Fe}^{2+}\text{-O}$

bonds, causing a restricted motion of the other bonds and lowering the position of the bands in samples with a higher Fe concentration (tab. 2).

Tab. 2 Raman bands and assignments of orthopyroxenes

| Enstatite | | Bronzite | | Hypersthene | | Assignments |
|---------------------|---------------------------|---------------------|---------------------------|---------------------|--|-----------------------------|
| Huang et al. (2000) | Present study Sample 5796 | Huang et al. (2000) | Present study Sample 5798 | Huang et al. (2000) | | |
| 239 | 234 | 234 | 228 | 229 | | |
| 304 | 296 | 297 | 290 | | | |
| 343 | 339 | 339 | 335 | 331 | | |
| 402 | 401 | 398 | 392 | 390 | | M-O stretch/bend |
| | | | | 406 | | |
| 421 | 440 | 439 | 427 | | | |
| 446 | 480 | | 454 | | | |
| 523 | 520 | 518 | 516 | 515 | | |
| 541 | 534 | 537 | 537 | 536 | | O-Si-O bend |
| 552 | 548 | 548 | 568 | 566 | | |
| 583 | 585 | | 581 | | | |
| 663 | 662 | 661 | 656 | 655 | | Si-O _{br} stretch |
| 686 | 681 | 682 | 674 | 675 | | |
| | 731 | | | | | |
| 750 | 750 | 748 | 745 | 748 | | |
| 854 | 858 | 858 | 870 | 868 | | |
| 933 | 928 | 938 | 939 | 936 | | |
| 1013 | 1010 | 1009 | 1003 | 1004 | | Si-O _{nbr} stretch |
| 1033 | 1027 | 1025 | | | | |
| | 1097 | | | 1013 | | |

Calcium pyroxenes

For clinopyroxenes, the group theory predicts 30 Raman modes: $14A_g + 16B_g$ (Rustein and White, 1971).

The spectra of diopside and hedenbergite (fig. 2) are also characterized by two intense bands, corresponding to the Si-O_{nbr} stretching mode (1010 cm^{-1} in diopside and 1012 cm^{-1} in hedenbergite) and to the stretching of Si-O_{br} bonds (665 cm^{-1} in diopside and 663 cm^{-1} in hedenbergite). In the $500\text{-}560\text{ cm}^{-1}$ region, bands assigned to the O-Si-O bending modes were observed, and in the lower region, bands attributed to the cation-oxygen vibrations (tab. 3).

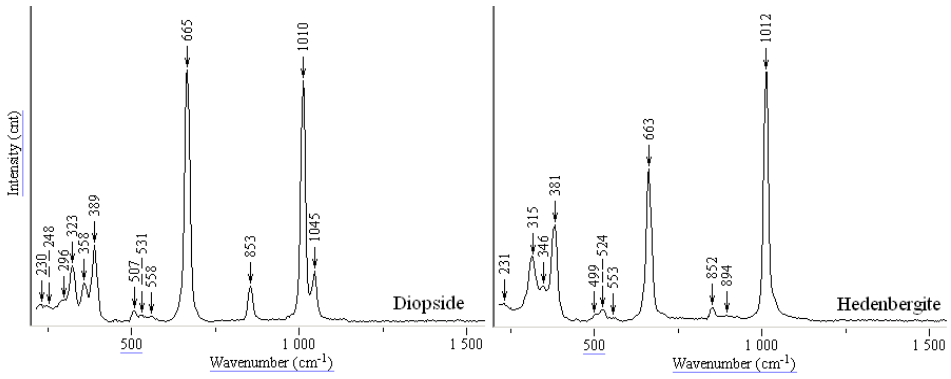


Fig. 2 Raman spectra of diopside and hedenbergite

Tab. 3 Raman bands and assignments of diopside and hedenbergite

| Diopside | | Hedenbergite | | | Assignments | |
|-----------------------|--------------|-----------------------|--------------|-------------|-------------|-----------------------------|
| Present study samples | Huang et al. | Present study samples | Huang et al. | (2000) | | |
| 5790 | 5791 | (2000) | 5792 | 5799 | (2000) | |
| 230 | 229 | 230 | | 231 | 233 | |
| 248 | 247 | 255 | 245 | | | |
| 296 | | | | | | |
| 323 | 323 | 325 | 315 | 315 | 307 | M-O stretch/bend |
| 358 | 359 | 359 | 346 | 346 | 338 | |
| 389 | 389 | 392 | 381 | 381 | 375 | |
| | | | | | 404 | |
| 507 | | 509 | | 499 | 495 | |
| 531 | 527 | 529 | 522 | 524 | 522 | O-Si-O bend |
| 558 | 560 | 558 | 555 | 553 | 549 | |
| 665 | 666 | 665 | 663 | 663 | 660 | Si-O _{br} stretch |
| | | | 758 | | 750 | |
| 853 | 852 | 854 | 853 | 852 | 853 | |
| | | | 890 | | | |
| | 907 | | 908 | 894 | 907 | Si-O _{nbr} stretch |
| 1010 | 1010 | 1011 | 1010 | 1012 | 1012 | |
| 1045 | 1045 | 1047 | 1036 | | 1031 | |

Huang et al. (2000) showed that with a constant Ca content most Raman bands in diopside-hedenbergite series should decrease with an increase of the Fe concentration. In all spectra from the present study, this observation is available only for the bands located in the 200-800 cm^{-1} region and for the peak from $\sim 1040 \text{ cm}^{-1}$; the $\sim 850 \text{ cm}^{-1}$ band preserves the same position, and the band at $\sim 1010 \text{ cm}^{-1}$ is slightly higher in hedenbergite (1010 cm^{-1} in diopside samples and 1012 cm^{-1} in hedenbergite sample 5799). The Raman spectra of diopside are similar to those reported in the literature (Etchepare, 1971; Swamy et al., 1997; Huang et al., 2000). The spectra of hedenbergite are different from those reported by Huang et al. (2000) (tab. 3), especially for the low region attributed to the cation-oxygen vibration modes. These differences are probably caused by a higher content of Mg in M1 sites in our studied samples.

In the Raman spectrum of augite (fig. 3), the stretching modes of Si-O_{nbr} are observed to have the highest intensity at 1006 cm^{-1} , and weaker peaks at 863 cm^{-1} , 928 cm^{-1} , 1043 cm^{-1} and 1102 cm^{-1} . The bands assigned to the stretching of the Si-O_{br} bonds are located at 667 cm^{-1} , 707 cm^{-1} and 769 cm^{-1} . The 533 cm^{-1} and 555 cm^{-1} bands are attributed to the bending of O-Si-O bonds. The cation-oxygen vibrations appear at lower frequencies, below 400 cm^{-1} (tab. 4).

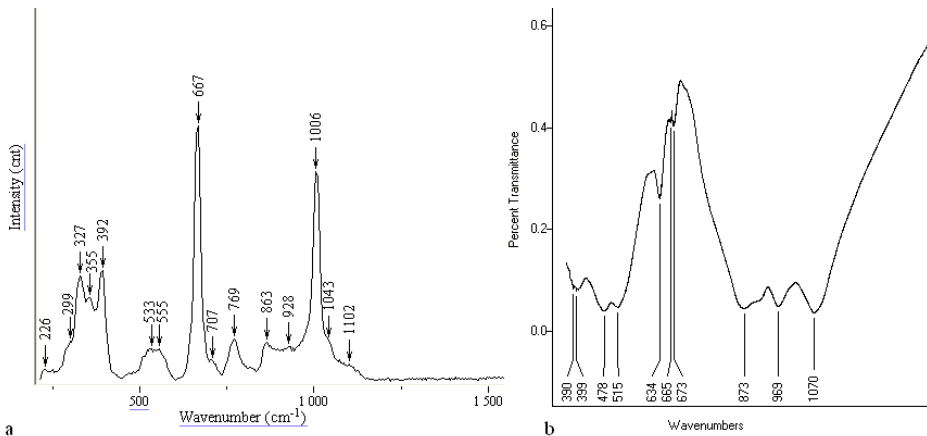


Fig. 3 Raman (a) and IR (b) spectra of augite

Based on the chemical composition of the augite specimens from the Techereu area (Apuseni Mountains, Romania), the formula resulting for this mineral is the following: $(\text{Ca}_{0.844}\text{Na}_{0.034}\text{K}_{0.009}\text{Mg}_{0.113})(\text{Mg}_{0.737}\text{Fe}^{3+}_{0.226}\text{Fe}^{2+}_{0.007}\text{Ti}_{0.014}\text{Al}_{0.014}\text{Mn}_{0.002})[(\text{Si}_{1.832}\text{Al}_{0.168})\text{O}_6]$ (tab. 5) (Stoicovici, 1968) The high content of Ca and Mg makes the augite from Techereu very similar to the diopside structure. The Raman spectrum of augite is also similar to the diopside spectrum (fig. 2). The bands in the low region of the augite and diopside Raman spectra are located at a maximum difference of 5 cm^{-1} ; the highest peak assigned to the stretching modes of Si-O_{nbr} is slightly lower in augite than in diopside (1006 cm^{-1} and

1010 cm^{-1} , respectively), caused probably by the Al content in the tetrahedral sites. More bands appear in the augite spectrum, at 707 cm^{-1} , 769 cm^{-1} and 1102 cm^{-1} . From the Raman spectra of the other augite sample studied (3974), it can be concluded that the specimen is also similar to diopside; a difference in the Raman spectra appears in the 700-1000 cm^{-1} region (tab. 4), where more bands are observed in augite than in diopside, probably due to the presence of a high Al content.

Tab. 4 Raman and infrared bands and assignments of augite

| Raman | | | | IR | | |
|-----------------------|-------------|---------------------|-----------------------------|--------------------------------------|------------------------|----------------------------|
| Present study samples | | Huang et al. (2000) | Assignments | Present study sample (from Techereu) | Makreski et al. (2006) | Assignments |
| from | 3974 | | | | | |
| Techereu | | | | | | |
| 226 | | | M-O stretch/bend | | | M-O stretch/bend |
| 299 | | | | | | |
| 327 | 324 | 323 | | | | |
| 355 | 352 | 352 | | 390 | 393 | |
| 392 | 389 | 387 | | 399 | | |
| | 477 | 461 | 478 | 469 | O-Si-O bend | |
| | | 508 | 515 | 521 | | |
| 533 | 532 | 531 | | | | |
| 555 | 555 | 556 | | 634 | 634 | O-Si-O bend |
| 667 | 663 | 662 | | 665 | | |
| | | | | 673 | 673 | |
| 707 | 714 | | Si-O _{nbr} stretch | | | Si-O _{br} stretch |
| 769 | 771 | 769 | | | | |
| | 816 | | | | | |
| 863 | 853 | 862 | | | | |
| | 878 | | | 873 | 872 | |
| | 896 | | | | 919 | |
| 928 | 924 | | | 969 | 974 | |
| 1006 | 1006 | 1007 | | | | |
| 1043 | 1037 | 1038 | | | | |
| 1102 | 1109 | | | | 1070 | |

The infrared spectrum of augite (fig. 3) revealed bands at frequencies of 87 cm^{-1} , 969 cm^{-1} and 1070 cm^{-1} , attributed to the stretching of the Si-O bonds (tab. 4); 1070 cm^{-1} is considered to be caused by the Si-O_{nbr} stretch, while the bands at smaller frequencies are assigned to the Si-O_{br} stretch. The bending modes are observed at 634 cm^{-1} , 665 cm^{-1} and 673 cm^{-1} . Below 520 cm^{-1} , the vibrations between cation and oxygen are presented as four bands: 390 cm^{-1} , 399 cm^{-1} , 478 cm^{-1} and 515 cm^{-1} . This assignment for IR bands of

augite was also made by Makreski et al. (2006).

Tab. 5 Chemical composition of augite minerals from the Techereu area, Romania (Stoicovici, 1968)

| Oxide | wt% | Cations calculated at 6 oxygen atoms | |
|--------------------------------|-------|--------------------------------------|-------|
| SiO ₂ | 48.42 | Si | 1.832 |
| TiO ₂ | 0.5 | Ti | 0.014 |
| Al ₂ O ₃ | 4.08 | Al | 0.182 |
| Fe ₂ O ₃ | 7.94 | Fe ³⁺ | 0.226 |
| FeO | 0.22 | Fe ²⁺ | 0.007 |
| MnO | 0.07 | Mn | 0.002 |
| MgO | 15.08 | Mg | 0.850 |
| CaO | 20.82 | Ca | 0.844 |
| K ₂ O | 0.19 | K | 0.009 |
| Na ₂ O | 0.46 | Na | 0.034 |
| LOI | 1.02 | O | 6 |
| H ₂ O | 0.38 | | |
| Total | 99.18 | | |

The group theory predicts for *c2/c* clinopyroxenes the following normal modes of vibration: 14A_g (R) + 16B_g (R) + 13A_u (IR) + 14B_u (IR) (Rustein and White, 1971). There are no modes which are Raman and IR active at the same time. An ideal SiO₄ tetrahedron has four fundamental modes: ν_1 symmetric stretching, ν_2 symmetric bending, ν_3 asymmetric stretching and ν_4 asymmetric bending. A large cation in the structure can distort the SiO₄ tetrahedra. This will make ν_1 and ν_2 Raman active, and ν_3 and ν_4 – IR active (Mills et al., 2005). In the case of our augite, we can assume that the Ca cation is producing the distortion and then the symmetric modes will be Raman active and the asymmetric ones will be IR active. Under these circumstances, the assignment made by Makreski et al. (2006) for the IR spectrum and ours for the Raman spectrum (tab. 4) are correct, based also on the rule that in SiO₄ tetrahedra $\nu_2 < \nu_4$ and $\nu_1 < \nu_3$ (Nakamoto, 2009).

Calcium-Sodium pyroxenes

The Raman spectrum of omphacite (fig. 4) reveals the characteristic bands of clinopyroxenes. The stretching modes of Si-O_{nbr} appear as five bands, with 1013 cm⁻¹ at the highest intensity, and the Si-O_{br} modes as one band at 667 cm⁻¹. The bending modes of Si-O bonds are observed in the 450-570 cm⁻¹ region as four bands. As in the other cases, below 400 cm⁻¹ are located the modes of the interactions between cation and oxygen (tab. 6).

The Raman spectrum reported by Downs (2006) is not comparable with that obtained in the present study (tab. 6). The measured chemistry of sample R061129 (Downs, 2006) is given by the formula (Ca_{0.51}Na_{0.49})(Mg_{0.43}Al_{0.42}Fe²⁺_{0.08}Fe³⁺_{0.07})[Si₂O₆]. Our Raman spectrum of omphacite is more similar to the diopside spectrum, which leads to the conclusion that our sample is characterized by a higher concentration of Ca and Mg.

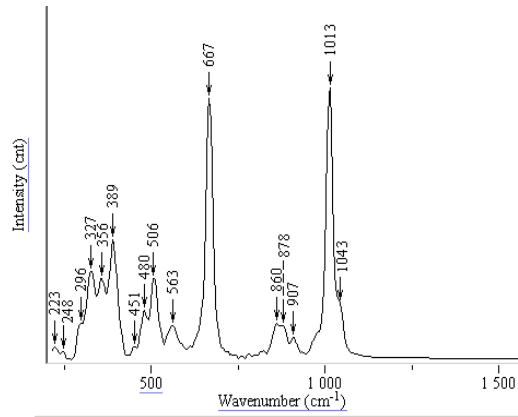


Fig. 4 Raman spectrum of omphacite

Tab. 6 Raman bands and assignments of omphacite

| Present study | Downs (2006) (R061129) | Assignments |
|---------------------|------------------------|-----------------------------|
| 223 | 217 | M-O stretch/bend |
| 248 | 264 | |
| 296 | | |
| 327 | | |
| 356 | 343 | |
| 389 | 376 | |
| 451 | | O-Si-O bend |
| 480 | 522 | |
| 506 | 558 | |
| 563 | 605 | Si-O _{br} stretch |
| 667 | 686 747 | |
| 860 | | Si-O _{nbr} stretch |
| 878 | | |
| 907 | 910 | |
| 1013 1043 | 1022 | |

Sodium pyroxenes

The Raman spectra of aegirine (fig. 5) are characterized by lower frequencies of the bands, compared with the rest of the clinopyroxenes. In the stretching region of Si-O_{nbr}, bands were observed at 866 cm⁻¹, 952 cm⁻¹, 971 cm⁻¹, 1041 cm⁻¹ and 1132 cm⁻¹ in the

5805 sample; and 866 cm^{-1} , 953 cm^{-1} , 1044 cm^{-1} and 1130 cm^{-1} in the 5820 sample. The stretching modes of Si-O_{br} are observed at 544 cm^{-1} , 678 cm^{-1} , ~757 cm^{-1} and a weak shoulder at 558 cm^{-1} in the 5805 sample. The bending modes of Si-O are located at ~466 cm^{-1} and ~497 cm^{-1} . Below 400 cm^{-1} , the bands are assigned to the vibrations of M-O bonds (tab. 7).

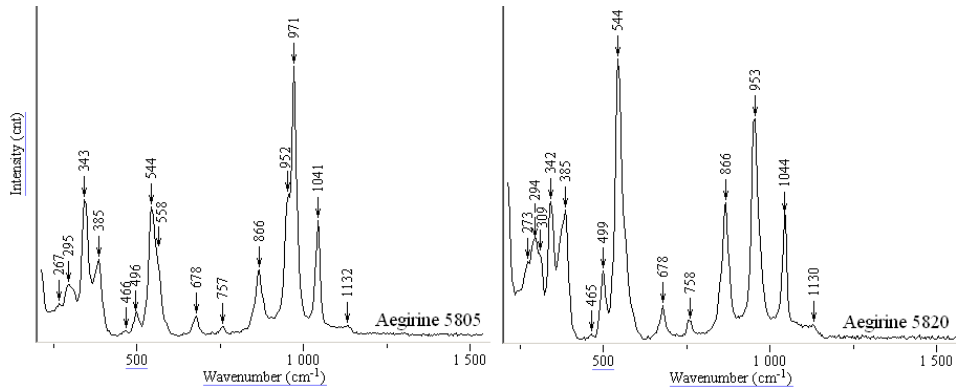


Fig. 5 Raman spectra of aegirine

Tab. 7 Raman bands and assignments of aegirine

| Aegirine | | | |
|------------------------------|------------------------------|---------------------------|----------------------------|
| Present study Sample 5820 | Present study Sample 5805 | Downs (2006) (R040054) | Assignments |
| 273 | 267 | 271 | |
| 294 | 295 | | |
| 309 | | 307 | |
| 342 | 343 | 341 | M-O stretch/bend |
| | | 363 | |
| 385 | 385 | 384 | |
| 465 | 466 | 465 | O-Si-O bend |
| 499 | 496 | 496 | |
| 544 | 544 | 545 | |
| | 558 | 562 | |
| 678 | 678 | 676 | Si-O _{br} stretch |
| 758 | 757 | 755 | |
| 866 | 866 | 865 | |
| 953 | 952 | 953 | |
| | 971 | 970 | Si-O _{nr} stretch |
| 1044 | 1041 | 1042 | |
| 1130 | 1132 | 1132 | |

In the spectrum of the 5805 sample (fig. 5), the higher intensity bands corresponding to the Si-O stretch are present as doublets. In the case of orthopyroxenes, these splits of the bands were attributed to the vibrations of two different tetrahedra. In aegirine, this is probably caused by the substitution of Na^+ with Ca^{2+} in the M2 sites, and implicitly, Fe^{3+} with Fe^{2+} in M1 sites. These substitutions lead to the distortion of the tetrahedra chain, creating two types of Si tetrahedra.

In the previous literature, no discussion on the Raman spectrum of aegirine was reported. A study on Li-aegirine ($\text{LiFeSi}_2\text{O}_6$) was made by Pommier et al. (2005) in order to follow the phase transition under pressure from the $C2/c$ to $P2_1/c$ structure.

Lithium pyroxenes

The spodumene Raman spectrum is shown in figure 6. The Raman bands characteristic for pyroxenes appear at higher frequencies in the spodumene spectrum. The bands corresponding to the Si-O_{nbr} vibrations are observed at 1017 cm^{-1} , 1070 cm^{-1} and 1098 cm^{-1} . The stretching modes of Si-O_{br} bonds are located at 705 cm^{-1} and 783 cm^{-1} . The bands attributed to O-Si-O bending in calcium pyroxene correspond to 522 cm^{-1} and 582 cm^{-1} in spodumene. Sharma and Simons (1981) assigned the 522 cm^{-1} band to the Al-O stretching mode of the AlO_6 group, together with 478 cm^{-1} and 438 cm^{-1} . The other bands from the low region of the spectrum are assigned to the cation-oxygen interactions (tab. 8).

A series of Raman studies were made on spodumene in order to follow the effects of phase transition from low ($C2/c$) to high ($P2_1/c$) pressure (Pommier et al., 2003).

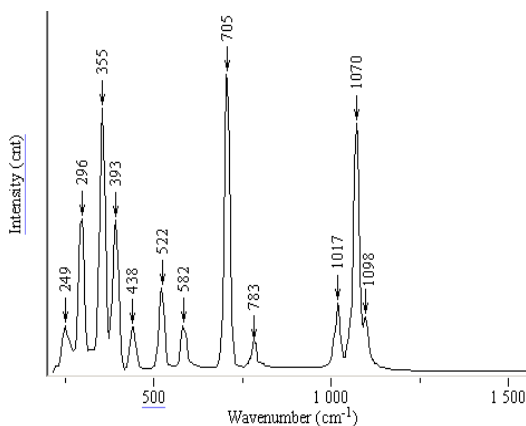


Fig. 6 Raman spectrum of spodumene

In all studied clinopyroxenes with a $C2/c$ structure, the Raman spectra have the same shape, showing bands of the characteristic vibrations: M-O modes, Si-O bending, Si-O_{br} stretching and Si-O_{nbr} stretching. The differences between minerals appear in the positions of these peaks. In the aegirine spectra (fig. 5), the bands assigned to the Si-O stretch are

observed at 544 cm^{-1} and $953\text{-}971\text{ cm}^{-1}$; in diopside, hedenbergite and augite (figs. 2 and 3), these bands appear at $\sim 665\text{ cm}^{-1}$ and $\sim 1010\text{ cm}^{-1}$, while in spodumene (fig. 6) – at 705 cm^{-1} and 1070 cm^{-1} . This shifting of the position of the bands from lower (aegirine) to medium (diopside, hedenbergite and augite) to higher frequencies (spodumene) appears to be related to the chemical composition in the M1 and M2 sites. The bands shift on higher wavenumbers with a decrease of the cation size in the M2 site, from Na^+ to Ca^{2+} to Li^+ . The high strength of M2-O bonds restricts the motion of Si-O bonds, making them vibrate at higher wavenumbers.

Tab. 8 Raman bands and assignments of spodumene

| Present study Sample 5876 | Sharma and Simons (1981) | Assignments |
|------------------------------|--------------------------|-----------------------------|
| | 225 | |
| 249 | 247 | |
| 296 | 296 | |
| | 326 | M-O stretch/bend |
| 355 | 356 | |
| 393 | 389 | |
| | 412 | |
| 438 | 436 | |
| 522 | 512 | |
| | 542 | O-Si-O bend |
| 582 | 583 | |
| | 614 | |
| 705 | 707 | |
| 783 | 782 | |
| | 884 | Si-O _{br} stretch |
| | 973 | |
| 1017 | 1012 | |
| 1070 | 1066 | Si-O _{nbr} stretch |
| 1098 | 1095 | |

Pyroxenoids

The Raman spectrum of wollastonite (fig. 7) is dominated by a strong fluorescence and the peaks are very weak and only a few can be distinguished clearly. The Si-O_{nbr} stretching modes are observed at 887 cm^{-1} , 968 cm^{-1} , 1042 cm^{-1} , 1097 cm^{-1} and 1133 cm^{-1} . For Si-O_{br}, the band at 635 cm^{-1} is assigned, and for the bending mode of Si-O – the 581 cm^{-1} band. The 338 cm^{-1} , 412 cm^{-1} and 502 cm^{-1} bands are attributed to Ca-O bending and stretching modes (tab. 9). Huang et al. (2000) had reported more Raman bands for wollastonite. All bands of wollastonite are different from pyroxene spectra.

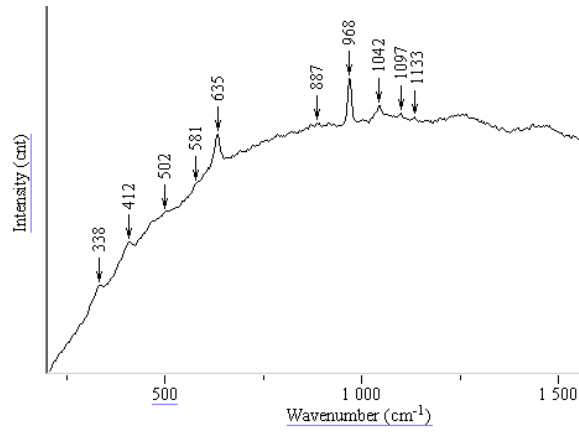


Fig. 7 Raman spectrum of wollastonite

Tab. 9 Raman bands and assignments of wollastonite

| Present study Sample 5734 | Huang et al. (2000) | |
|------------------------------|---------------------|-----------------------------|
| | 226 | |
| | 237 | |
| | 257 | |
| | 303 | M-O stretch/bend |
| | 321 | |
| 338 | 337 | |
| | 400 | |
| 412 | 412 | |
| 502 | 485 | |
| 581 | 581 | O-Si-O bend |
| 635 | 636 | Si-O _{br} stretch |
| | 688 | |
| 887 | 883 | |
| 968 | 970 | |
| | 997 | |
| | 1020 | Si-O _{nbr} stretch |
| 1042 | 1044 | |
| 1097 | | |
| 1133 | | |

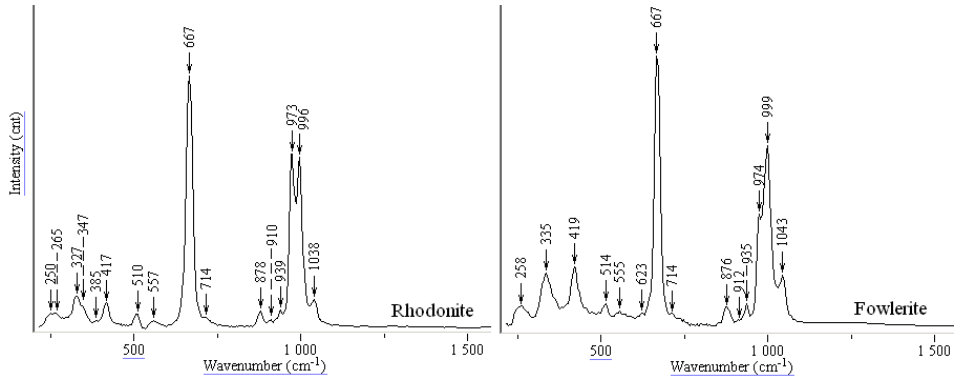


Fig. 8 Raman spectra of rhodonite and fowlerite

The Raman spectra of rhodonite and fowlerite are shown in figure 8. Fowlerite is the zinc-rich variety of rhodonite, with the formula $(\text{Mn,Zn})\text{SiO}_3$. In the $870\text{--}1045\text{ cm}^{-1}$ region, the modes of Si-O_{nbr} bonds are observed, the highest band appearing as a doublet at $\sim 973\text{ cm}^{-1}$ and $\sim 997\text{ cm}^{-1}$, caused by the structure of rhodonite, where the five repeating tetrahedra of SiO_4 have different Si-O bond lengths. The region assigned in the pyroxenes to the stretching modes of the Si-O_{br} bonds is present in the rhodonite spectra at 667 cm^{-1} . No splitting of this peak is observed; weak bands appear at 714 cm^{-1} , and an additional one in fowlerite at 623 cm^{-1} . The bending modes of O-Si-O are observed at 510 cm^{-1} and 557 cm^{-1} in rhodonite, and 514 cm^{-1} and 555 cm^{-1} in fowlerite. The cation-oxygen vibration modes appear in the low region of the spectra below 420 cm^{-1} (tab. 10). There are some differences in the Raman spectra of the studied samples. The stretching modes of Si-O_{nbr} are slightly shifted on higher frequencies in fowlerite, except for the $\sim 877\text{ cm}^{-1}$ and $\sim 937\text{ cm}^{-1}$ bands. This behaviour is also observed for the bending modes. In the region of the M-O modes, the bands at 250 cm^{-1} and 265 cm^{-1} in rhodonite appear in fowlerite as a single one at 258 cm^{-1} ; the band at 327 cm^{-1} in rhodonite is observed at 335 cm^{-1} in fowlerite. The presence of Zn in fowlerite is causing these changes; a smaller size of Zn compared with Ca is creating stronger bonds, producing the shifting of the bands on higher wavenumbers in fowlerite.

Only a few studies were made on charoite (Rogova et al., 1978; Rozhdestvenskaya et al., 2009). Downs (2006) reported Raman spectra for charoite that are similar to the spectrum obtained in the present study; no discussions or band assignments for this mineral were found in the literature.

As in the case of wollastonite, the Raman spectrum of charoite (fig. 9) is characterized by a strong fluorescence and background noise and the peaks are very weak and only a few can be distinguished. The structure of this mineral is still not clear, so an assignment of the bands is difficult to achieve. Like the other silicates which contain chains of SiO_4 tetrahedra, we can assume that the 638 cm^{-1} , 675 cm^{-1} , 1054 cm^{-1} , 1116 cm^{-1} and 1135 cm^{-1} peaks are

due to the Si-O bending/stretching modes. In the region of the M-O vibrations, the bands are very weak and only 242 cm^{-1} and 434 cm^{-1} were observed. In the high region of the spectrum, two new lines were observed at 2367 cm^{-1} and 2403 cm^{-1} . Weinstein et al. (2001) reported these Raman bands for the vibrations of the N-H bonds in gallium nitride samples implanted with H^+ . It is possible that charoite contains NH_4^+ ions in its structure, through the substitution of K^+ atoms.

Tab. 10 Raman bands and assignments of rhodonite and fowlerite

| Present study Rhodonite 5760 | Present study Fowlerite 5745 | Mills et al. (2004) | Assignments |
|---------------------------------|---------------------------------|---------------------|-----------------------------|
| | | 217 | |
| 250 | | 247 | |
| 265 | 258 | 263 | |
| | | 277 | |
| | | 298 | |
| 327 | | 321 | |
| | 335 | 337 | |
| 347 | | 346 | M-O stretch/bend |
| | | 360 | |
| 385 | | 386 | |
| | | 390 | |
| 417 | 419 | 416 | |
| | | 435 | |
| | | 455 | |
| | | 473 | |
| | | 495 | |
| 510 | 514 | 513 | |
| | | 543 | O-Si-O bend |
| 557 | 555 | 556 | |
| | | 570 | |
| | 623 | | |
| 667 | 667 | 667 | Si-O _{br} stretch |
| | | 680 | |
| 714 | 714 | 715 | |
| | | 737 | |
| 878 | 876 | 878 | Si-O _{nbr} stretch |
| 910 | 912 | 915 | |
| 939 | 935 | 936 | |
| 973 | 974 | 974 | |
| | | 989 | |
| 996 | 999 | 999 | |
| | | 1011 | |
| 1038 | 1043 | 1052 | |

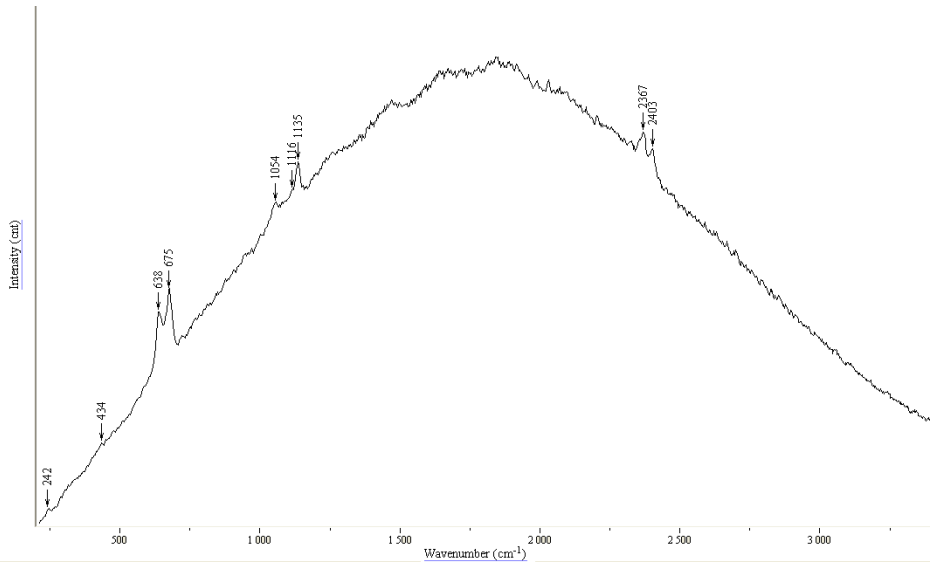


Fig. 9 Raman spectrum of charoite

Conclusions

Three types of vibrations in pyroxenes and pyroxenoids were observed in all spectra devised for the present study, namely M-O modes, Si-O bending and Si-O stretching modes. These vibrations are present at different wavenumbers, depending on the structure and chemical composition.

In orthopyroxenes (enstatite-ferrosilite), the bands decrease in frequency with the increasing of the Fe concentration from enstatite to ferrosilite, caused by the greater size of the Fe^{2+} cation, compared with the Mg^{2+} one. The Mg^{2+} cation is forming stronger bonds, restricting the motion of the other bonds and making them vibrate at higher frequencies.

In all studied clinopyroxenes with a $C2/c$ structure, the Raman spectra have the same shape. The shifting of the position of the bands from lower (aegirine) to medium (diopside, hedenbergite and augite) to higher frequencies (spodumene) appears to be related to the chemical composition in the M1 and M2 sites. The bands shift on higher wavenumbers with a decrease of the cation size in the M2 site, from Na^+ to Ca^{2+} to Li^+ . The high strength of M2-O bonds restricts the motion of Si-O bonds, making them vibrate at higher wavenumbers.

The IR spectrum of augite completed the vibrational modes of this pyroxene. From the assignment made for the Raman and IR bands results that the symmetric modes are Raman active and the asymmetric ones are IR active, due to a distortion of the SiO_4 tetrahedra caused by a large cation in the structure, Ca in our case.

Despite the twisted and deformed SiO₄ chains in the pyroxenoids, the Raman spectra are similar to those of the pyroxenes, showing the same characteristic type of vibration modes.

Acknowledgments

This work was supported by CNCSIS –UEFISCSU, project number PNII – IDEI code 2119/2008

References

- Chopelas, A., 1999. Estimates of mantle relevant Clapeyron slopes in the MgSiO₃ system from high-pressure spectroscopic data. *American Mineralogist*, **84**, 233–244.
- Deer, W.A., Howie, R.A., Zussman, J., 1997. *Rock-forming Minerals*. Vol. 2A, Single-chain Silicates. Second edition. The Geological Society, London.
- Downs, R.T., 2006. The RRUFF Project: an integrated study of the chemistry, crystallography, Raman and infrared spectroscopy of minerals. Program and Abstracts of the 19th General Meeting of the International Mineralogical Association in Kobe, Japan. (www.rruff.info).
- Etchepare, J., 1971. Study by Raman spectroscopy of crystalline and glassy diopside. In: Douglas, R.W., Ellis, B. (Eds.), *Amorphous materials*. Wiley Interscience, London, 337–346.
- Huang, E., Chen, C.H., Huang, T., Lin, E.H., Xu, J., 2000. Raman spectroscopic characteristics of Mg-Fe-Ca pyroxenes. *American Mineralogist*, **85**, 473–479.
- Katerinopoulou, A., Musso, M., Amthauer, G., 2008. A Raman spectroscopic study of the phase transition in omphacite. *Vibrational Spectroscopy*, **48**, 163–167.
- Makreski, P., Jovanovski, G., Gajović, A., Biljan, T., Angelovski, D., Jačimović, R., 2006. Minerals from Macedonia. XVI. Vibrational spectra of some common appearing pyroxenes and pyroxenoids. *Journal of Molecular Structure*, **788**, 102–114.
- McMillan, P., 1984. Structural studies of silicate glasses and melts-applications and limitations of Raman spectroscopy. *American Mineralogist*, **69**, 622–644.
- Mernagh, T.P., Hoatson, D.M., 1997. Raman Spectroscopic Study of Pyroxene Structures from the Munni Munni Layered Intrusion, Western Australia. *Journal of Raman Spectroscopy*, **28**, 647–658.
- Mills, S.J., Frost, R.L., Kloprogge, J.T., Weier, M.L., 2005. Raman spectroscopy of the mineral rhodonite. *Spectrochimica Acta, Part A*, **62**, 171–175.
- Nakamoto, K., 2009. *Infrared and Raman Spectra of Inorganic and Coordination Compounds, Part A: Theory and Applications in Inorganic Chemistry* (Sixth edition). John Wiley and Sons, New Jersey.
- Pommier, C.J.S., Denton, M.B., Downs, R.T., 2003. Raman spectroscopic study of spodumene (LiAlSi₂O₆) through the pressure-induced phase change from *C2/c* to *P21/c*. *Journal of Raman Spectroscopy*, **34**, 769–775.
- Pommier, C.J.S., Downs, R.T., Stimpfl, M., Redhammer, G.J., Denton, M.B., 2005. Raman and X-ray investigations of LiFeSi₂O₆ pyroxene under pressure. *Journal of Raman Spectroscopy*, **36**, 864–871.
- Rogova, V.P., Rogov, Y.G., Drits, V.A., Kuznetsova, N.N., 1978. Charoite, a new mineral, and a new jewelry stone. *Zapiski Vsesoyuznogo Mineralogicheskogo Obschestva*, **107**, 94–100. (In Russian).
- Rozhdestvenskaya, I.V., Kogure, T., Abe, E., Drits, V.A., 2009. A structural model for charoite. *Mineralogical Magazine*, **73/5**, 883–890.
- Rutstein, M.S., White, W.B., 1971. Vibrational spectra of high-calcium pyroxenes and pyroxenoids. *American Mineralogist*, **56**, 877–887.
- Sharma, S.K., Simons, B., 1981. Raman study of crystalline polymorphs and glasses of spodumene composition quenched from various pressures. *American Mineralogist*, **66**, 118–126.
- Sharma, S.K., Simons, B., Yoder, H.S., 1983. Raman study of anorthite, calcium Tschermak's pyroxene, and gehlenite in crystalline and glassy states. *American Mineralogist*, **68**, 1113–1125.

- Stoicovici, E., 1968. The augite in the diabase from Techerău (Hunedoara). *Bul. Soc. de Șt. Geol.*, **XI**, 203–211. (In Romanian).
- Swamy, V., Dubrovinsky, L.S., Matsui, M., 1997. High-temperature Raman spectroscopy and quasi-harmonic lattice dynamic simulation of diopside. *Phys. Chem. Minerals*, **24**, 440–446.
- Wang, A., Joliff, B.L., Haskin, L.A., Kuebler, K.E., Viskupic, K.M., 2001. Characterization and comparison of structural and compositional features of planetary quadrilateral pyroxenes by Raman spectroscopy. *American Mineralogist*, **86**, 790–806.
- Weinstein, M.G., Jiang, F., Stavola, M., Nielsen, B.B., Usui, A., Mizuta, M., 2001. Hydrogen vibrational lines in HVPE GaN. *Physica B*, 308–310, 122–125.

Received: April, 2010

Revised: May, 2010

Accepted: June, 2010